The Millimeter Wave Rotational Spectrum of N-Cyanomethanimine, CH2NCN

ARTICLE *in* JOURNAL OF MOLECULAR SPECTROSCOPY · MAY 1984

Impact Factor: 1.48 · DOI: 10.1016/0022-2852(84)90111-5

3 AUTHORS, INCLUDING:

Curt Wentrup
University of Queensland

576 PUBLICATIONS **6,481** CITATIONS

SEE PROFILE

JOURNAL OF MOLECULAR SPECTROSCOPY **105**, 193–205 (1984)

The Millimeter Wave Rotational Spectrum of *N*-Cyanomethanimine, CH_2NCN

MANFRED WINNEWISSER AND BRENDA P. WINNEWISSER

Physikalisch-Chemisches Institut, Justus-Liebig-Universität, Giessen, Heinrich-Buff-Ring 58, 6300 Giessen, West Germany

AND

CURT WENTRUP

Fachbereich Chemie, Philipps-Universität, Marburg, West Germany

The rotational spectrum of the short-lived species *N*-cyanomethanimine, CH_2NCN, has been measured in the frequency range 100–250 GHz. The observed transitions allow the determination of the rotational and centrifugal distortion constants and the nitrogen quadrupole coupling constants for both nitrogen nuclei. The *N*-cyanomethanimine spectrum was measured directly in the products of the pyrolysis of trimethylenetetrazole. The rotational constants obtained are A = 63 372.995(11) MHz, B = 5 449.347 90(28) MHz, and C = 5 009.559 86(29) MHz; the quadrupole coupling constants are χ_{aa} = 2.057(39) MHz and $\chi_{bb} - \chi_{cc} = -7.205(21)$ MHz for the imine nitrogen, and $\chi_{aa} = -3.264(33)$ MHz and $\chi_{bb} - \chi_{cc} = -1.630(18)$ MHz for the cyano-group nitrogen. The accurate constants obtained allow the calculation of the line position and hyperfine structure of any rotational transition appropriate for a radioastronomical search.

INTRODUCTION

Since HCN is a rather abundant interstellar molecule, there is a growing interest in the various chemical dimers of HCN, exemplified by the recent *ab initio* study of Dykstra *et al.* (*1*). None of the dimers of HCN are stable in the laboratory, and only two have been identified so far in the vapor phase; the linear van der Waals dimer (*2–4*) and *N*-cyanomethanimine, H_2CNCN. The first experimental detection of *N*-cyanomethanimine, by Wentrup (*5*), was in the products of a gas-phase pyrolysis of trimethylenetetrazole, where mass spectrometry data indicated that one of the products was *N*-cyanomethanimine (*5*). Meanwhile, this has been confirmed using low-temperature infrared spectroscopy by Wentrup and Lorencak (*6*). Another pyrolysis precursor, dimethylcyanamide, was shown by Bak *et al.* (*7*) to also yield *N*-cyanomethanimine. They were able to measure microwave transitions of both normal and deuterated *N*-cyanomethanimine (*7, 8*), and could thus determine the dipole moment components and a partial substitution structure (*8, 9*) which agrees rather well with the *ab initio* structure given in (*1*).

Because of the possible interstellar interest of the molecule, we undertook to extend the measurement of the rotational spectrum into the millimeter wave range and try to find the *b*-type spectrum. Similar studies of the related molecules acrylonitrile

0022-2852/84 $3.00

(vinyl cyanide), CH_2CHCN (*10*), and isocyanoethene (vinyl isocyanide), CH_2CHNC (*11*), had previously been made in this laboratory, in which both *a*- and *b*-type rotational transitions were measured. At the time our millimeter wave work was begun, Bak and co-workers had been able to identify only *a*-type transitions. Following an exchange of information between the two laboratories, the *b*-type spectrum could be found both in the microwave (*9*) and millimeter wave regions.

Nuclear quadrupole hyperfine splitting due to both nitrogen nuclei, which contributed to very broad lines in the microwave work, could be resolved in the millimeter wave spectrum. The present report therefore includes the measurement and analysis of the hyperfine structure in the millimeter wave rotational spectrum of *N*-cyanomethanimine.

EXPERIMENTAL PROCEDURES

The pyrolysis precursor, trimethylenetetrazole, was prepared as described in Ref. (*5*). About 100 mg of trimethylenetetrazole was placed in a small Pyrex finger attached to a quartz pyrolysis tube, 2 cm in diameter, which led into the absorption cell of the spectrometer over a pyrex pathway of about 50 cm. The precursor was warmed to 50–70°C, giving a vapor pressure of about 0.5 Pa, and the quartz tube was heated in an oven held at 500°C. The pyrolysis products expanded directly into an absorption cell with a volume of about 20 liters, and were pumped either continuously at a slow rate or intermittently. The half-life of *N*-cyanomethanimine in the cell was approximately 10 min. The strongest lines could be observed on the oscilloscope in the video mode, without signal averaging, at total pressures of 0.1–0.2 Pa. The only other products identified in Ref. (*5*) were N_2 and ethylene, as indicated in Fig. 1. Indeed, no absorptions other than those of *N*-cyanomethanimine were observed in the millimeter wave spectrum.

The millimeter wave spectrometer (*12, 13*) uses harmonic multiplication of microwave klystron radiation to generate millimeter wave power, and a helium-cooled InSb chip as detector. The detector and the sweep stabilization of the free-running klystron are described in Ref. (*14*). Most of the rotational transitions of *N*-cyanomethanimine were measured with computer averaging of the detected signal in the fast sweep mode, but the eight lines whose hyperfine structures were analyzed in detail were recorded with source modulation and phase stabilization of the klystron as described in Ref. (*15*). In the latter case the second harmonic of the reference

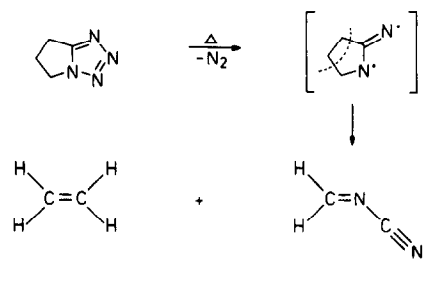

FIG. 1. Reaction scheme for the gas-phase pyrolysis of trimethylenetetrazole at 500°C and 1 Pa (*5*).

frequency was taken for the phase-sensitive detection, so that a second-derivative line shape was obtained. The modulation frequency was 3.2 kHz.

ROTATIONAL STRUCTURE

From the low-J, a-type lines observed by Bak *et al.* (*7*), and with centrifugal distortion constants taken from acrylonitrile (*10*), the a-type transitions in the frequency range 100–300 GHz were predicted. The typical pattern for a-type transitions of a slightly asymmetric rotor could then easily be identified. The lines for $K_a = 3$ to 8 in each J transition form a bandhead, as shown in Fig. 2 for $J = 20$–19. After fitting the first few lines, it was possible to follow the a-type transitions up to $J = 25$ and $K_a = 16$. Only the highest K_a lines for $J = 9$ to 13 showed broadening or splitting due to quadrupole coupling, as is discussed below.

On the basis of the a-type transitions, a least-squares fit was made to refine those constants which determine the a-type transition frequencies, and a prediction of the b-type transitions was made. The $K_a = 2$ inertial asymmetry splitting gave a good determination of the linear combination $A - D_K$, but the distortion constant D_K remained undetermined. Our predictions for the b-type transitions were thus uncertain by roughly $D_K K_a^2$, and D_K was expected to be of the order of 2–10 MHz. The region where we sought likely candidates in the b-type spectrum was sprinkled with a-type transitions in excited vibrational states which were stronger than the b-type lines turned out to be. As shown in Ref. (*9*), the b component of the dipole moment is only ~1.5 Debye, whereas the a component is 4.6 Debye. In addition, as we soon discovered, the b-type lines were much more affected by quadrupole splitting than the a-type lines, reducing their peak intensity and thus making them even more

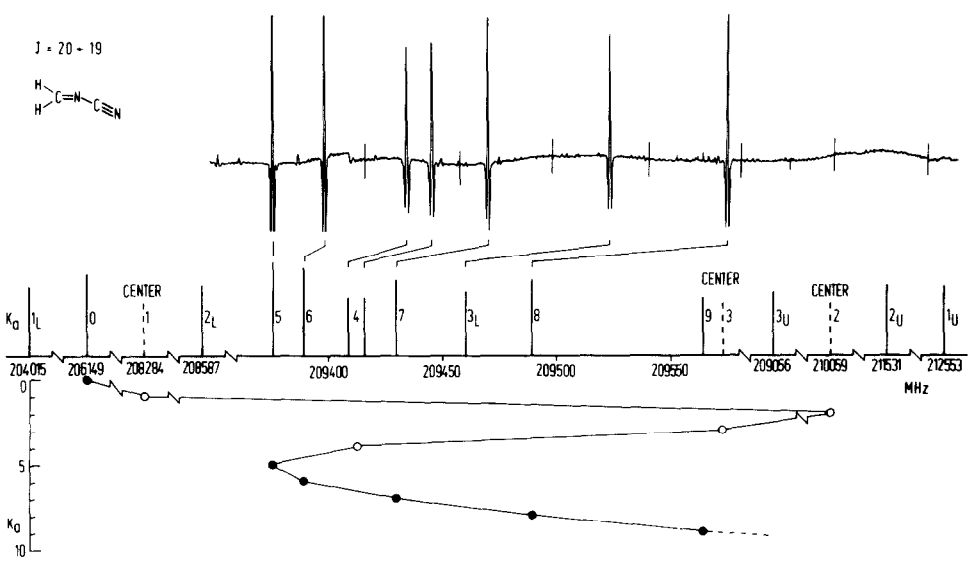

FIG. 2. A typical bandhead in the a-type spectrum of CH_2NCN. The second derivative of the spectrum was recorded with source modulation in the 6th harmonic of the klystron frequency. The frequency markers are separated by 23.4 MHz.

difficult to find; only later could we use the splitting to confirm assignments. In the microwave region, where the identification of lines is somewhat less difficult than in the millimeter wave region, Bak and Svanholt (*9*) were able to use constants refined from our data together with a calculated D_K value to identify eight *b*-type lines. On the basis of their assignment we were able to confirm a tentative assignment of the distinctive ${}^RQ_1$ bandhead at 146 GHz. A Fortrat diagram showing the very similar ${}^RQ_1$ bandhead of isocyanoethene is given in Ref. (*11*), Fig. 2. Due to the collapse of the hyperfine pattern at the bandhead, the lines are more intense than other *b*-type lines. It was then possible to go on to identify other *b*-type lines, including the lower ${}^RQ_2$ bandhead.

Our initial least-squares fit to the *a*- and *b*-type transitions together was very unsatisfactory; the large deviations revealed the magnitude of the quadrupole hyperfine structure of most of the *b*-type lines. Whereas the *b*-type lines of acrylonitrile are only broadened by the hyperfine interaction in the millimeter wave range, the lines of *N*-cyanomethanimine are split by as much as 2.5 MHz in this region.

Following the hyperfine analysis discussed in the next section, the calculated hyperfine structure was plotted for all of the lines which had been measured with signal averaging, and a correction was introduced, where necessary, for the deviation between the observed absorption maximum and the unsplit line center.

The list of rotational line centers given in Table I was then fitted to Watson's *S*-reduced rotational Hamiltonian (*16*), extended by two higher-order constants (*17*) required to fit the very high J and K values represented in the data:

$$\begin{aligned}\hat{H}_{\text{rot}} = {} & 1/2(B+C)\hat{P}^2 + \{A - 1/2(B+C)\}\hat{P}_a^2 - D_J(\hat{P}^2)^2 - D_{JK}\hat{P}^2\hat{P}_a^2 - D_K\hat{P}_a^4 \\ & + \{(B-C)/4 + d_1\hat{P}^2\}(\hat{P}_+^2 + \hat{P}_-^2) + d_2(\hat{P}_+^4 + \hat{P}_-^4) + H_J(\hat{P}^2)^3 \\ & + H_{JK}(\hat{P}^2)^2\hat{P}_a^2 + H_{KJ}\hat{P}^2\hat{P}_a^4 + H_K\hat{P}_a^6 + h_1(\hat{P}^2)^2(\hat{P}_+^2 + \hat{P}_-^2) + h_2\hat{P}^2(\hat{P}_+^4 + \hat{P}_-^4) \\ & + h_3(\hat{P}_+^6 + \hat{P}_-^6) - L_{JK}(\hat{P}^2)^2\hat{P}_a^4 - L_{KJ}\hat{P}^2\hat{P}_a^6. \quad (1)\end{aligned}$$

The operators $\hat{P}$, $\hat{P}_a$, $\hat{P}_+ = \hat{P}_x + i\hat{P}_y$, and $\hat{P}_- = \hat{P}_x - i\hat{P}_y$ are the total angular momentum and its components, respectively, in the principal axis system. The adjusted rotational and centrifugal distortion constants are listed in Table II and compared with those of acrylonitrile. The magnitude of the centrifugal distortion constants indicate that *N*-cyanomethanimine is quite rigid. The lines reported by Bak and co-workers (*7, 9*) were omitted from the fit because of the large deviations found between the observed and calculated values. These deviations are easily explained by the calculated quadrupole splitting, which varies between 0 and 2 MHz among these lines, and by the wall broadening and pressure broadening in a microwave cell at the higher pressures apparently required in the pyrolysis of dimethylcyanamide. For six of the eight *b*-type lines reported in Ref. (*9*), corrections estimated from plotting the hyperfine pattern account for all but ca. 50 kHz of the deviation.

QUADRUPOLE HYPERFINE STRUCTURE

The two nitrogen nuclei are labeled N(1) and N(2) in Fig. 3, which shows the molecule in its inertial axis system. Since both nitrogen nuclei contribute substantially to the observed hyperfine structure, the hyperfine patterns were calculated by determining the first-order hyperfine energy for two nuclei. The computer programs to

TABLE I

Observed and Calculated Rotational Transitions (in MHz) of *N*-Cyanomethanimine in the Ground Vibrational State

$J'(K_a',K_c')$-$J''(K_a'',K_c'')$	OBSERVED	CALCULATED	OBS-CALC	$J'(K_a',K_c')$-$J''(K_a'',K_c'')$	OBSERVED	CALCULATED	OBS-CALC
a-type transitions				20(8,13)-19(8,12)	209489.5412	209489.5455	-0.0043
(Q)R(K)				20(9,12)-19(9,11)	209564.0336	209564.0275	0.0061
1(0, 1)- 0(0, 0)		10458.8982		20(10,11)-19(10,10)	209651.1078	209651.1091	-0.0013
				20(11,10)-19(11, 9)	209749.4374	209749.4427	-0.0053
2(0, 2)- 1(0, 1)	20915.2900	20915.2432	0.0468 a	20(12, 9)-19(12, 8)	209858.1307	209858.1267	0.0040
2(1, 2)- 1(1, 1)	20479.3500	20478.4859	0.8641 a	20(13, 8)-19(13, 7)	209976.5128	209976.5013	0.0115
2(1, 1)- 1(1, 0)	21357.4800	21358.0309	-0.5509 a				
				21(0,21)-20(0,20)	216201.2842	216201.2752	0.0090
3(0, 3)- 2(0, 2)	31366.5200	31366.4834	0.0366 a	21(1,21)-20(1,20)	214144.1763	214144.1817	-0.0054
3(1, 3)- 2(1, 2)	30716.3000	30716.0580	0.2420 a	21(1,20)-20(1,19)	223056.0569	223056.0846	-0.0277
3(1, 2)- 2(1, 1)	32035.2200	32035.3085	-0.0885 a	21(2,20)-20(2,19)	218949.7673	218949.7671	0.0002
3(2, 2)- 2(2, 1)	31380.6900	31379.5827	1.1073 a	21(2,19)-20(2,18)	222285.7518	222285.7589	-0.0071
3(2, 1)- 2(2, 0)	31388.3100	31389.5576	-1.2476 a	21(3,19)-20(3,18)	219945.1397	219945.1463	-0.0066
				21(3,18)-20(3,17)	220232.8198	220232.8124	0.0074
10(0,10)- 9(0, 9)	104171.5617	104171.5624	-0.0007	21(4,18)-20(4,17)	219894.4866	219894.4839	0.0027
10(1,10)- 9(1, 9)	102288.8254	102288.8235	0.0019	21(4,17)-20(4,16)	219903.2821	219903.3017	-0.0196
10(1, 9)- 9(1, 8)	106675.8277	106675.8458	-0.0181	21(5,17)-20(5,16)	219851.3910	219851.3220	0.0690 d
10(2, 9)- 9(2, 8)	104526.9238	104526.9426	-0.0188	21(5,16)-20(5,15)	219851.3910	219851.4606	-0.0696 d
10(2, 8)- 9(2, 7)	104934.5847	104934.5775	0.0072	21(6,16)-20(6,15)	219860.4066	219860.4095	-0.0029 c
10(3, 8)- 9(3, 7)	104655.3716	104655.3663	0.0053	21(6,15)-20(6,14)	219860.4066	219860.4108	-0.0042 c
10(3, 7)- 9(3, 6)	104662.3334	104662.3437	-0.0103	21(7,14)-20(7,13)	219900.3923	219900.3964	-0.0041
10(4, 7)- 9(4, 6)	104652.7085	104652.6822	0.0263 c	21(8,13)-20(8,12)	219961.2777	219961.2638	0.0139
10(4, 6)- 9(4, 5)	104652.7085	104652.7267	-0.0182 c	21(9,12)-20(9,11)	220038.2340	220038.2588	-0.0248
10(5, 6)- 9(5, 5)	104665.5244	104665.5155	0.0089	21(10,11)-20(10,10)	220128.8317	220128.8247	0.0070
10(6, 5)- 9(6, 4)	104688.3076	104688.3079	-0.0003	21(11,10)-20(11, 9)	220231.3744	220231.4252	-0.0508
10(7, 4)- 9(7, 3)	104718.3695	104718.2923	0.0772 e	21(12, 9)-20(12, 8)	220345.0411	220345.0248	0.0163
10(8, 3)- 9(8, 2)	104754.4163	104754.3180	0.0983 f	21(13, 8)-20(13, 7)	220468.9442	220468.9343	0.0099
10(9, 2)- 9(9, 1)	104795.7957	104795.8009	-0.0052 g	21(14, 7)-20(14, 6)	220602.5335	220602.5292	0.0043
				21(15, 6)-20(15, 5)	220745.3604	220745.3499	0.0105
13(0,13)-12(0,12)		135068.4049					
13(1,13)-12(1,12)		132884.1603		25(0,25)-24(0,24)	256236.2764	256236.2870	-0.0106
13(1,12)-12(1,11)	138566.5222	138566.5266	-0.0044	25(1,25)-24(1,24)	254582.4823	254582.4904	-0.0081
13(2,12)-12(2,11)	135814.6319	135814.6343	-0.0024	25(1,24)-24(1,23)	264845.4870	264845.4954	-0.0084
13(2,11)-12(2,10)	136700.1314	136700.1294	0.0020	25(2,24)-24(2,23)	260305.2974	260305.2962	0.0012
13(3,11)-12(3,10)	136081.2588	136081.2569	0.0019	25(2,23)-24(2,22)	265358.5290	265358.5290	0.0000
13(3,10)-12(3, 9)	136107.6146	136107.6124	0.0022	25(3,23)-24(3,22)	261875.6925	261875.6892	0.0033
13(4,10)-12(4, 9)	136064.6180	136064.4634	0.1546 d	25(3,22)-24(3,21)	262546.3397	262546.3303	0.0094
13(4, 9)-12(4, 8)	136064.6180	136064.7590	-0.1410 d	25(4,22)-24(4,21)	261851.9677	261851.9687	-0.0010
13(5, 9)-12(5, 8)	136071.9630	136071.9561	0.0069 c	25(4,21)-24(4,20)	261881.7632	261881.7561	0.0071
13(5, 8)-12(5, 7)	136071.9630	136071.9577	0.0053 c	25(5,21)-24(5,20)	261761.7330	261761.7092	0.0238
13(6, 8)-12(6, 7)	136096.7052	136096.7090	-0.0038	25(5,20)-24(5,19)	261762.3670	261762.3819	-0.0149
13(7, 7)-12(7, 6)	136132.8079	136132.7997	0.0082	25(6,20)-24(6,19)	261747.8809	261747.8804	0.0005 c
13(8, 6)-12(8, 5)	136177.7874	136177.7734	0.0140	25(6,19)-24(6,18)	261747.8809	261747.8896	-0.0087 c
13(9, 5)-12(9, 4)	136230.4327	136230.4283	0.0044	25(7,19)-24(7,18)	261780.8029	261780.8106	-0.0077
13(10, 4)-12(10, 3)	136289.4029	136290.0775	-0.6746 f	25(8,18)-24(8,17)	261843.8432	261843.8412	0.0020
13(11, 3)-12(11, 2)	136356.2669	136356.2702	-0.0033 g	25(9,17)-24(9,16)	261929.0648	261929.0518	0.0130
				25(10,16)-24(10,15)	262032.2346	262032.2373	-0.0027
14(0,14)-13(0,13)	145299.0233	145299.0174	0.0059	25(11,15)-24(11,14)	262150.9067	262150.9209	-0.0142
14(1,13)-13(1,12)	149176.9615	149176.9666	-0.0051	25(12,14)-24(12,13)	262283.5053	262283.5036	0.0017
14(1,14)-13(1,13)	143068.8397	143068.8441	-0.0044	25(13,13)-24(13,12)	262428.8694	262428.8650	0.0044
14(2,13)-13(2,12)	146232.3240	146232.3285	-0.0045	25(14,12)-24(14,11)	262586.1923	262586.1614	0.0309
14(2,12)-13(2,11)	147330.5350	147330.5357	-0.0007	25(15,11)-24(15,10)	262754.7392	262754.7294	0.0097
14(3,12)-13(3,11)	146560.1147	146560.1134	0.0013	25(16,10)-24(16, 9)	262933.9505	262933.9765	-0.0260
14(3,11)-13(3,10)	146598.3870	146598.3799	0.0071	b-type transitions			
14(4,11)-13(4,10)	146537.6648	146537.6426	0.0222	(R)Q(0)			
14(4,10)-13(4, 9)	146538.1142	146538.1446	-0.0304	18(1,17)-18(0,18)	104068.9720	104068.9878	-0.0158 g
14(5,10)-13(5, 9)	146541.8891	146541.8811	0.0080 c	19(1,18)-19(0,19)	110026.2298	110026.2200	0.0098 g
14(5, 9)-13(5, 8)	146541.8891	146541.8844	0.0047 c	24(1,23)-24(0,24)	146525.3910	146525.3889	0.0021 g
14(6, 9)-13(6, 8)	146566.4767	146566.4856	-0.0089	(R)R(0)			
14(7, 8)-13(7, 7)	146604.1427	146604.1367	0.0060	14(1,14)-13(0,13)	183805.3316	183805.3436	-0.0120 g
14(8, 7)-13(8, 6)	146651.7975	146651.7874	0.0101	19(1,19)-18(0,18)	223328.6900	223328.6885	0.0015 h
14(9, 6)-13(9, 5)	146707.9669	146707.9572	0.0097	(R)P(1)			
14(10, 5)-13(10, 4)	146771.8265	146771.8101	0.0164	8(0, 8)- 7(1, 7)	31223.0400	31223.4585	-0.4185 b
14(11, 4)-13(11, 3)	146842.8122	146842.8077	0.0050	14(0,14)-13(1,13)	104562.4983	104562.5179	-0.0196 g
14(12, 3)-13(12, 2)	146920.6225	146920.5283	0.0642 e	(R)Q(1)L			
14(13, 2)-13(13, 1)	147004.7428	147004.7527	-0.0099 h	18(2,16)-18(1,17)	149753.3380	149753.3529	-0.0149 h
				19(2,17)-19(1,18)	148511.5310	148510.9007	0.6303 f
17(0,17)-16(0,16)	175847.5140	175847.5065	0.0075	20(2,18)-20(1,19)	147489.0100	147489.0048	0.0052 h
17(1,17)-16(1,16)	173577.5468	173577.5392	0.0076	21(2,19)-21(1,20)	146718.6720	146718.6791	-0.0071 h
17(1,16)-16(1,15)	180933.7739	180933.7737	0.0002	22(2,20)-22(1,21)	146229.3770	146229.3742	0.0028
17(2,16)-16(2,15)	177444.5746	177444.5658	0.0088	23(2,21)-23(1,22)	146048.8232	146048.8240	-0.0008
17(2,15)-16(2,14)	179348.2210	179348.2059	0.0151	24(2,22)-24(1,23)	146202.9723	146202.9787	-0.0064
17(3,15)-16(3,14)	178005.7617	178005.7402	0.0215	25(2,23)-25(1,24)	146716.0190	146716.0123	0.0067 h
17(3,14)-16(3,13)	178106.8512	178106.8456	0.0056	26(2,24)-26(1,25)	147610.4200	147610.3868	0.0332 h
17(4,14)-16(4,13)	177966.2102	177966.1749	0.0353	27(2,26)-27(1,26)	148906.9250	148906.9477	-0.0227 h
17(4,13)-16(4,12)	177968.1357	177968.1670	-0.0313	(R)Q(1)U			
17(5,13)-16(5,12)	177955.5911	177955.5973	-0.0062 c	9(2, 8)- 9(1, 9)	184344.9920	184344.9505	0.0415 h
17(5,12)-16(5,11)	177955.5911	177955.6174	-0.0263 c	(R)R(1)L			
17(6,11)-16(6,10)	177976.9184	177976.9045	0.0139	5(2, 4)- 4(1, 3)	224450.5530	224450.6072	-0.0542 h
17(7,10)-16(7, 9)	178017.5888	178017.5470	0.0418	(R)P(1)L			
17(8, 9)-16(8, 8)	178072.1431	178072.1416	0.0015	11(2,10)-12(1,11)	32123.0800	32122.6031	0.4769 b
17(9, 8)-16(9, 7)	178138.0896	178138.1118	-0.0222	17(1,16)-16(2,15)	35562.6800	35563.1072	-0.4272 b
17(10, 7)-16(10, 6)	178213.9865	178214.0417	-0.0552	22(1,21)-21(2,20)	107202.9885	107203.0061	-0.0176 g
17(11, 6)-16(11, 5)	178299.0715	178299.0527	0.0188	(R)P(1)U			
17(12, 5)-16(12, 4)	178392.5496	178392.5374	0.0122	16(2,14)-17(1,17)	38693.1500	38693.9902	-0.8402 b
17(13, 4)-16(13, 3)	178493.9899	178494.0348	-0.0449	17(2,15)-18(1,18)	34309.9600	34310.8507	-0.8907 b
17(14, 3)-16(14, 2)	178603.1920	178603.1681	0.0239	18(2,16)-19(1,19)	30492.9400	30493.6522	-0.7122 b
17(15, 2)-16(15, 1)	178719.6146	178719.6122	0.0024	19(2,17)-20(1,20)	27266.4400	27267.2938	-0.8538 b
				(R)Q(2)L			
18(0,18)-17(0,17)	185973.7573	185973.7534	0.0039	41(3,38)-41(2,39)	223568.9312	223568.9496	-0.0184
18(1,18)-17(1,17)	183731.3456	183731.3454	0.0002	42(3,39)-42(2,40)	222784.0175	222784.0160	0.0015
18(2,17)-17(2,16)	187833.5860	187833.5930	-0.0070	43(3,40)-43(2,41)	222428.1902	222428.1728	0.0174
				44(3,41)-44(2,42)	222526.6109	222526.5997	0.0112
20(2,19)-19(2,18)	208586.6038	208586.5863	0.0175	45(3,42)-45(2,43)	223102.2133	223102.2214	-0.0081
20(3,18)-19(3,17)	209460.0101	209460.0085	0.0016	46(3,43)-46(2,44)	224175.7439	224175.7491	-0.0052
20(3,17)-19(3,16)	209686.3105	209686.3008	0.0097	(R)P(3)U			
20(4,17)-19(4,16)	209409.7342	209409.7168	0.0174	9(3, 6)-10(2, 9)	186112.3800	186112.3521	0.0279
20(4,16)-19(4,15)	209415.9929	209415.9783	0.0146	13(3,10)-14(2,13)	145244.8653	145244.8907	-0.0254
20(5,16)-19(5,15)	209376.1861	209376.1134	0.0727 d	(R)P(3)L			
20(5,15)-19(5,14)	209376.1861	209376.2023	-0.0162 d	9(3, 7)-10(2, 8)	184876.3700	184876.9003	-0.5303 f
20(6,15)-19(6,14)	209389.1903	209389.1860	0.0043 c	22(3,20)-23(2,21)	29632.8700	29632.9092	-0.0392 b
20(6,14)-19(6,13)	209389.1903	209389.1868	0.0035 c	37(2,35)-36(3,34)	185302.6920	185302.6909	0.0011 h
20(7,14)-19(7,13)	209429.8971	209429.8906	0.0065				

[a] From Ref. (7); given zero weight.
[b] From Ref. (9); given zero weight.
[c] Unresolved doublet; each line given weight 0.5.
[d] Partially resolved doublet; given zero weight.
[e] Uncorrected quadrupole shift; given zero weight.
[f] Overlap of excited state line or bad measurement; given zero weight.
[g] Exact quadrupole analysis; see text and Table III.
[h] Graphical quadrupole correction; see text.

TABLE II

Rotational and Centrifugal Distortion Constants of *N*-Cyanomethanimine[a] and Acrylonitrile[b] in the *S*-Reduced Rotational Hamiltonian for the Ground Vibrational State

	CH_2NCN	CH_2CHCN
A/MHz	63 372.995 3(115)	49 850.698 2(87)
B/MHz	5 449.347 90(28)	4 971.164 06(70)
C/MHz	5 009.559 86(29)	4 513.877 20(76)
D_J/kHz	2.394 66(58)	2.182 1(17)
D_{JK}/kHz	-129.900 2(59)	-85.076(18)
D_K/kHz	5 786.6(35)	2 717.1(11)
d_1/kHz	-0.485 46(20)	-0.457 14(58)
d_2/kHz	-0.032 994(64)	-0.030 53(20)
H_J/Hz	0.006 27(43)	0.004 4(13)
H_{JK}/Hz	-0.297 0(71)	-0.343(26)
H_{KJ}/Hz	-27.417(46)	-7.09(12)
H_K/Hz	1 486.(260)	433.(37)
h_1/Hz	0.002 45(16)	0.002 90(71)
h_2/Hz	0.000 330(85)	-0.000 12(38)
h_3/Hz	0.000 117(32)	0.000 146(48)
L_{JK}/Hz	0.000 307(34)	
L_{KJ}/Hz	-0.009 31(15)	
No. of lines	150	129
σ/kHz	17	44

[a]This work.

[b]The data of Ref. (10) was refitted to the S-reduced Hamiltonian.

carry out this calculation and do a least-squares adjustment of the coupling constants were made available to us by H. Günther, University of Tübingen (*18*). The programs calculate the matrix elements

$$\langle \Phi | \hat{H}_Q | \Phi' \rangle$$

$$= \frac{1}{4}(-1)^{F'_1+J+I_1+I}\delta_{F_1F'_1}\frac{\begin{Bmatrix} F'_1 & I_1 & J \\ 2 & J & I_1 \end{Bmatrix}}{\begin{pmatrix} I_1 & 2 & I_1 \\ -I_1 & 0 & I_1 \end{pmatrix}\begin{pmatrix} J & 2 & J \\ -J & 0 & J \end{pmatrix}} D(1) + \frac{1}{4}(-1)^{F+F_1+F'_1-J+I_1+I_2+1}$$

$$\times [(2F'_1+1)(2F_1+1)]^{1/2}\frac{\begin{Bmatrix} F & I_2 & F'_1 \\ 2 & F_1 & I_2 \end{Bmatrix}\begin{Bmatrix} I & J & F'_1 \\ 2 & F_1 & J \end{Bmatrix}}{\begin{pmatrix} I_2 & 2 & I_2 \\ -I_2 & 0 & I_2 \end{pmatrix}\begin{pmatrix} J & 2 & J \\ -J & 0 & J \end{pmatrix}} D(2) \qquad (2)$$

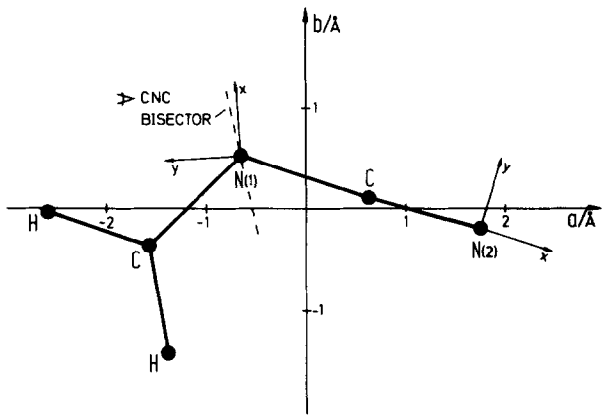

FIG. 3. CH_2NCN in its inertial axis system, based on the *ab initio* structure (Ref. (*1*)). The auxiliary axis systems shown are the principal axis systems of the *ab initio* quadrupole coupling tensors (Ref. (*20*)) for the two nitrogen nuclei.

in the basis

$$|\Phi\rangle = |(JI_1)F_1I_2FM_F\rangle,$$

where

$$D(i) = \frac{2}{(J+1)(2J+3)}\{\chi_{aa}^{(i)}(\langle\hat{P}_a^2\rangle - \langle\hat{P}_c^2\rangle) + \chi_{bb}^{(i)}(\langle\hat{P}_b^2\rangle - \langle\hat{P}_c^2\rangle)\}, \qquad i = 1, 2. \quad (3)$$

The $\chi_{\alpha\alpha}^{(i)}$ are the diagonal tensor elements of the quadrupole coupling tensor in the inertial axis system, and the $\langle\hat{P}_\alpha^2\rangle$ are the expectation values of the square of the rotational angular momentum operators. The coupling scheme used is $J + I_1 = F_1$ and $F_1 + I_2 = F$. The notation used in the definitions of $|\Phi\rangle$ and Eq. (2) are explained in Ref. (*19*). The matrix of $\hat{H}_Q$ is diagonalized and treated as a first-order perturbation to the rotational energy. A plotting routine was added for generating a Gaussian line shape or the first or second derivative thereof. Such plots allow a direct comparison of calculated spectra with recorded spectra.

The starting point for analyzing the *N*-cyanomethanimine quadrupole structure was acrylonitrile. The cyanide nitrogen N(2) of *N*-cyanomethanimine was expected to have coupling tensor components roughly similar to those of the nitrogen atom in acrylonitrile. It was further found that for the high-*J*, near-symmetric-top transitions observed, the splitting of the *a*-type transitions depends only on the χ_{aa} component of the two coupling tensors, and the splitting of the *b*-type transitions depends only on the differences $\chi_{bb} - \chi_{cc}$.

Eight lines showing large and characteristic hyperfine splitting were recorded at approximately Doppler broadening (ca. 0.2 Pa) with source modulation, in order to have a well-defined (second-derivative) line shape. The hyperfine coupling constants were adjusted empirically until a qualitative fit of splitting patterns was achieved. The measured splittings of these eight lines were then put into a least-squares adjustment. However, the spectra are only partly resolved, so that the observed absorption maxima do not correspond to individual hyperfine components. Ideally, a whole-line least-squares adjustment should be made. In the present case, we plotted the

calculated spectra, measured the distance between the calculated maxima and the individual hyperfine components, and added these corrections to the data for the least-squares fit. Since each measured maximum provides only one data point in this procedure, one calculated component was selected from each clump for the least-squares fit, generally a line showing large Jacobian matrix elements for the adjustment of the coupling constants. Table III summarizes the data used. Actually, the minimum information needed to obtain the four determinable constants is contained in the two transitions reproduced in Fig. 4. The two splitting intervals in the $10_{9,1}$–$9_{9,0}$ transition determine the two χ_{aa} values. The splitting between the pair of doublets in the $24_{1,23}$–$24_{0,24}$ transition determine the difference $\chi_{bb} - \chi_{cc}$ for one nucleus, and the doublet splitting itself determines the difference for the other. The set of four constants determined is unique in both sign and magnitude. As can be deduced by inspection of the small shoulder in the $10_{9,1}$–$9_{9,1}$ transition, the line width is very critical in reproducing the shape of the absorption features. A discrete least-squares procedure does not help here, and the line width was adjusted empirically on the more isolated features in each transition. A good reproduction of the shoulders in all of the *a*-type transitions in Table III was required. Thus, the fitting of the splittings required several iterations to optimize the line widths and the corrections, before the fit shown in Fig. 4 was attained.

The four coupling constants obtained are unique. However, ambiguities remain because it is possible (i) to associate each difference $\chi_{bb} - \chi_{cc}$ with either value of χ_{aa}, leading to quite different sets of individual components χ_{bb} and χ_{cc} since $\chi_{aa} + \chi_{bb} + \chi_{cc} = 0$ for each nucleus; and (ii) to associate either set of χ's with each of the two nitrogen nuclei. Table IV compares the hyperfine tensor components obtained in the two cases and those obtained for acrylonitrile. The standard errors

TABLE III

Measured Components (in MHz) of Selected Rotational Transitions of CH_2NCN Split by Quadrupole Hyperfine Interaction

$J'_{K_aK_c'} - J''_{K_aK_c''}$	Unperturbed frequency	Observed maxima	Calculated components[a]	F_1' F' – F_1'' F''
a-type transitions				
$10_{9,2} - 9_{9,1}$	104 795.7957	-0.5281	-0.5552	9 9 – 8 8
			-0.5054	11 11 – 10 10b
		-0.1882c	-0.1755	10 10 – 9 9
		0.0734	0.0263	9 10 – 8 9
			0.0590	11 12 – 10 11
			0.0874	9 8 – 8 7b
			0.1528	11 10 – 10 9
		0.4721	0.4216	10 11 – 9 10b
			0.4997	10 9 – 9 8
$13_{11,3} - 12_{11,2}$	136 356.2669	-0.3792	-0.3721	12 12 – 11 11b
			-0.3466	14 14 – 13 13
		0.0628	-0.1096	13 13 – 12 12
			0.0231	12 13 – 11 12
			0.0418	14 15 – 13 14b
			0.0562	12 11 – 11 10
			0.0879	14 13 – 13 12
		--c	0.2918	13 14 – 12 13
			0.3316	13 12 – 12 11
b-type transitions				
$14_{0,14} - 13_{1,13}$	104 562.4983	-0.3611	-0.4315	13 12 – 12 11
			-0.4056	13 14 – 12 13
			-0.3578	15 14 – 14 13b
			-0.3405	15 16 – 14 15
			-0.2174	13 13 – 12 12
			-0.1495	15 15 – 14 14
		0.5798	0.5507	14 13 – 13 12
			0.5738	14 15 – 13 14b
			0.7563	14 14 – 13 13
$14_{1,14} - 13_{0,13}$	183 805.3316	-0.6672	-0.8221	14 14 – 13 13
			-0.6144	14 15 – 13 14b
			-0.6048	14 13 – 13 12
		0.3647	0.1605	15 15 – 14 14
			0.2323	13 13 – 12 12
			0.3778	15 16 – 14 15b
			0.3812	15 14 – 14 13
			0.4461	13 14 – 12 13
			0.4591	13 12 – 12 11
$18_{1,17} - 18_{0,18}$	104 068.9720	-0.7794	-0.8488	17 16 – 17 16b
			-0.8303	17 18 – 17 18
			-0.7516	19 18 – 19 18
			-0.7217	19 20 – 19 20
		-0.3278	-0.3927	17 17 – 17 17b
			-0.2898	19 19 – 19 19
		1.1217	1.1075	18 17 – 18 17b
			1.1317	18 19 – 18 19
		1.5734	1.5750	18 18 – 18 18b
$19_{1,18} - 19_{0,19}$	110 026.229B	-0.8036	-0.8642	18 17 – 18 17b
			-0.8459	18 19 – 18 19
			-0.7694	20 19 – 20 19
			-0.7409	20 21 – 20 21
		-0.3291	-0.3998	18 18 – 18 18b
			-0.3000	20 20 – 20 20
		1.1432	1.1344	19 18 – 19 18b
			1.1578	19 20 – 19 20
		1.6131	1.6090	19 19 – 19 19b
$24_{1,23} - 24_{0,24}$	146 525.3910	-0.8773	-0.9214	23 22 – 23 22b
			-0.9052	23 24 – 23 24
			-0.8389	25 24 – 25 24
			-0.8152	25 26 – 25 26
		-0.3356	-0.4253	23 23 – 23 23b
			-0.3391	25 25 – 25 25
		1.2386	1.2361	24 23 – 24 23b
			1.2561	24 25 – 24 25
		1.7682	1.7397	24 24 – 24 24b
$22_{1,21} - 21_{2,20}$	107 202.9885	-0.4765	-0.5061	21 20 – 20 19b
			-0.4997	21 22 – 20 21
			-0.4619	23 22 – 22 21
			-0.4417	23 24 – 22 23
		-0.2100	-0.2598	21 21 – 20 20
			-0.2086	23 23 – 22 22b
		0.7065	0.6995	22 21 – 21 20b
			0.7118	22 23 – 21 22
		0.9925	0.9586	22 22 – 21 21b

[a]All listed components have at least 73% of the intensity of the strongest component in each transition.

[b]Components used in fit. Standard deviation was 8 kHz.

[c]Shoulder; not used in least squares fit.

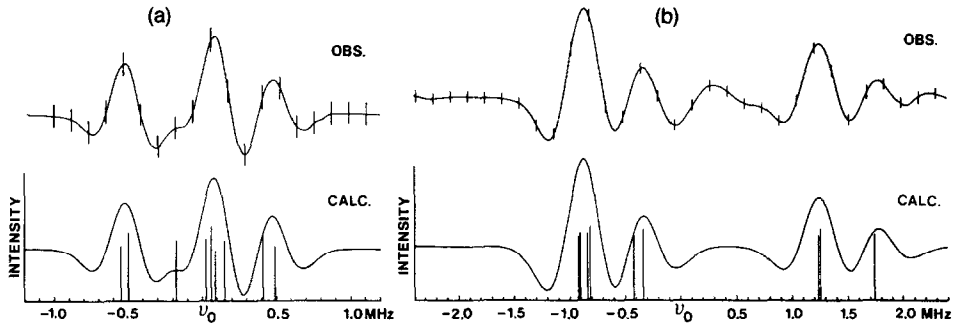

FIG. 4. Observed and calculated second derivative of the hyperfine structure of (a) an *a*-type and (b) a *b*-type transition in the millimeter wave spectrum of *N*-cyanomethanimine. The frequency markers in the observed transitions are separated by 117 kHz in (a) and 156 kHz in (b). The stick diagrams give the intensity and line position of the components, for which the quantum numbers are listed in Table III. (a) CH_2NCN, $J_{K_a'} = 10_9$–9_9, ν_0 = 104 795.7970 MHz; (b) CH_2NCN, $J_{K_a',K_c'} = 24_{1,23}$–$24_{0,24}$, ν_0 = 146 525.3954 MHz.

quoted are from the least-squares fit, and are perhaps optimistic measures of the true errors for this type of spectrum. The second ambiguity, which tensor is to be associated with which nitrogen nucleus, has been resolved in Table IV by requiring a similarity between the χ_{aa}'s of the cyano-nitrogen N(2) in *N*-cyanomethanimine and acrylonitrile.

TABLE IV

^{14}N Quadrupole Coupling Tensor Components (in MHz) in the Inertial Principal Axis Systems of *N*-Cyanomethanimine and Acrylonitrile

		CH_2NCN			CH_2CHCN
		Experimental[a]		Ab initio[b]	Experimental[c]
		Solution 1	Solution 2		
N(1):	χ_{aa}	2.057(39)	2.057	2.123	
	χ_{bb}	-4.631	-1.844	-3.899	
	χ_{cc}	2.574	-0.214	1.776	
	$\chi_{bb} - \chi_{cc}$	-7.205(21)	-1.630	-5.675	
N(2):	χ_{aa}	-3.264(33)	-3.264	-2.362	-3.69(5)
	χ_{bb}	0.817	-1.971	0.627	-0.53
	χ_{cc}	2.447	5.234	1.736	4.22
	$\chi_{bb} - \chi_{cc}$	-1.630(18)	-7.205	-1.109	-4.75(19)

[a]This work. The standard errors of the determinable components are given in parentheses in units of the last significant figure.
[b]Ref. (20).
[c]Ref. (10).

This is possible because the two molecules have similar orientations in their inertial principal axis systems, so that the χ tensor associated with the C=N bond may be assumed to have a similar orientation. The use of this same argument to resolve the first ambiguity fails because the χ_{bb} and χ_{cc} values for acrylonitrile fall just between the values found for solutions 1 and 2 in Table IV for N(2). Low-J, $K_a = 1$ lines are predicted to have different hyperfine patterns for the two solutions, but b-type lines in this category are very weak in the millimeter wave region, and the corresponding a-type lines in the microwave region are difficult to observe under high resolution. The choice was made by considering the *ab initio* electric field gradient tensor q at each nitrogen nucleus, made available by Jasien and Dykstra (*20*), together with the known structure. Because further results of the *ab initio* calculations were used, the *ab initio* structure given in Ref. (*1*) and reproduced in Fig. 3 was taken for purposes of interpretation of the χ tensors rather than the partial r_s structure of Ref (*9*).

The hyperfine coupling tensors $\chi = eqQ$ were obtained from the field gradient tensors q of Jasien and Dykstra by taking the nuclear quadrupole moment Q to be 0.0156×10^{-24} cm^2 (*21*). The resulting tensors were diagonalized to give the principal components and the principal axis system of each tensor. These axis systems are shown in Fig. 3, and the principal components are listed in Table V. The axis system of $\chi^{(2)}$ is just 2° from the C≡N bond, while the axis system of $\chi^{(1)}$ is displaced 8.8° from the CNC angle bisector, representing the nitrogen lone pair. The rotation necessary to transform the *ab initio* tensors from the arbitrary axis system to the inertial axis system could also be determined, and the calculated diagonal tensor components in this axis system are listed in Table IV together with our experimental values. The

TABLE V

Principal Components[a] (in MHz) of the ^{14}N Quadrupole Coupling Tensors in *N*-Cyanomethanimine

		Experimental[b]		Ab initio[c]
		Solution 1	Solution 2	
N(1):	χ_{xx}	-4.654	-1.865	-3.9315
	χ_{yy}	2.086	2.078	2.1549
	χ_{zz}	2.574	0.214	1.7764
	$\eta = \frac{\chi_{yy} - \chi_{zz}}{\chi_{xx}}$	0.105	-0.999	-0.096
N(2):	χ_{xx}	-3.680	-3.396	-2.6663
	χ_{yy}	1.233	-1.839	0.9307
	χ_{zz}	2.447	5.234	1.7356
	$\eta = \frac{\chi_{yy} - \chi_{zz}}{\chi_{xx}}$	0.330	2.083	0.302

[a]The axes were defined by diagonalization of the ab initio χ tensors. See Fig. 3.

[b]This work.

[c]Ref. (20).

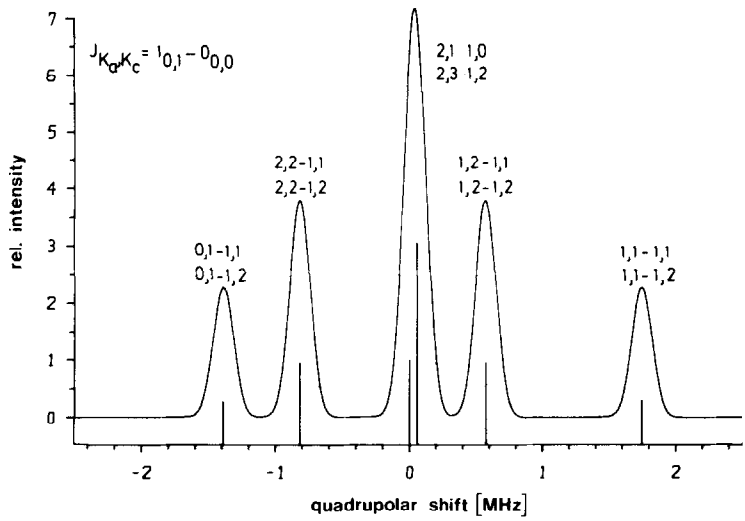

FIG. 5. Calculated hyperfine splitting of the as yet unobserved $1_{0,1}$–$0_{0,0}$ transition of CH_2NCN at 10 458.8982 MHz (calculated standard deviation = 0.5 kHz). The line shape is Gaussian, with a line width parameter of 100 kHz. The quantum numbers shown for the components are F_1', $F' - F_1''$, F''. From left to right, the five pairs of components are predicted to lie at −1.391, −0.818, 0.044, 0.576, and 1.748 MHz from the line center. The stick diagram should actually indicate twice as much intensity for all but the central pair, because they are degenerate.

similarity between the values found for solution 1 and the *ab initio* values allows us to choose solution 1 as the correct solution. This choice is further confirmed by rotating the experimental values, which are obtained in the inertial principal axis system, to their principal axis systems (*22*), assumed to be those of the *ab initio* χ tensors. The difference between the theoretical and true axis systems should be small enough to be negligible in this discussion. The components thus obtained are listed in Table V together with the eigenvalues of the *ab initio* tensors. We can now look at the asymmetry, $\eta = (\chi_{yy} - \chi_{zz})/\chi_{xx}$, of each coupling tensor in its principal axis system, which is a measure of the cylindrical symmetry of the electron distribution around the x axis (and is independent of the nuclear quadrupole moment Q). If solution 1 is taken, the experimental values of η agree satisfactorily with the *ab initio* values. However, if solution 2 is taken, the magnitude of both asymmetries is equal to or greater than 1, which would be at variance with any remotely cylindrical electronic distribution in the bonds under consideration. This circumstance would suffice to eliminate solution 2. Although this latter criterion is based on the experimental data alone, the experimental η values could be evaluated more reliably with the support of the theoretical structure and χ tensors.

CONCLUSION

The coupling constants as given in Table IV can be used to predict the hyperfine splitting in any rotational transition of *N*-cyanomethanimine. Plots were made of the predicted pattern of all the lines measured, and corrections were introduced to give the line center for most of the lines measured with the averaging technique, as men-

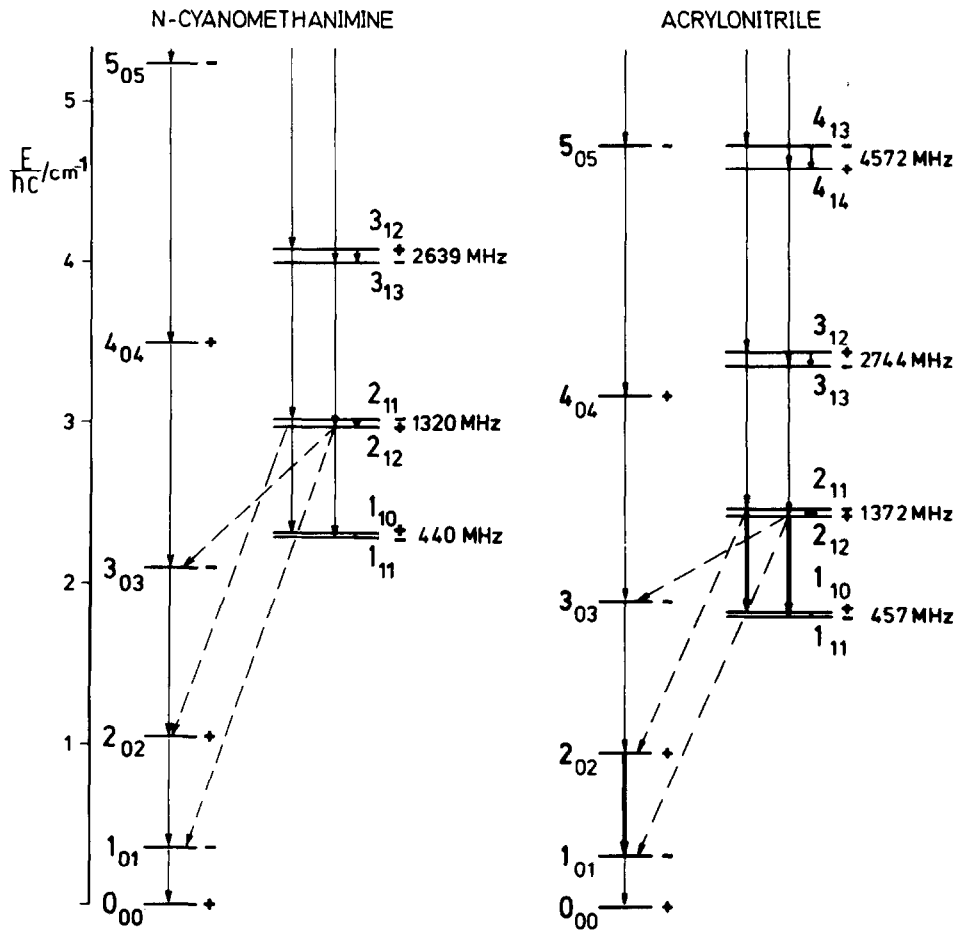

FIG. 6. Part of the rotational energy level diagram for CH_2NCN and CH_2CHCN showing possible interstellar transitions. For CH_2CHCN four transitions, entered as heavy arrows, have been observed in interstellar sources (Refs. (*23, 24*)).

tioned above. For the information of radioastronomers, the calculated hyperfine pattern of the 1_{01}–0_{00} transition is shown in Fig. 5. Upon request, the corresponding pattern for any other transition can be supplied by the authors. Such patterns are quite distinctive, and would suffice to identify a single interstellar line. Figure 6 shows part of the rotational energy level diagram of *N*-cyanomethanimine and acrylonitrile. Four of the five observed interstellar transitions of acrylonitrile (*23, 24*) fall in the region shown and have been entered as heavy lines. The same transitions for *N*-cyanomethanimine can be considered opportune for a radioastronomical search for this molecule.

ACKNOWLEDGMENTS

The authors would like to express their thanks to Dr. H. Günther for making his quadrupole programs available to us, and Dr. P. G. Jasien and Dr. C. E. Dykstra for sending us their hyperfine coupling constants

derived from *ab initio* calculations. The programming help of J. Reinstädtler is appreciated. The experimental work in Giessen and Marburg was supported by funds of the respective universities, the Deutsche Forschungsgemeinschaft, and the Fonds der Chemischen Industrie. The work in Giessen was also supported by the Max Planck Institute for Radioastronomy, Bonn. All calculations were carried out at the Hochschulrechenzentrum of the Justus Leibig University, Giessen.

RECEIVED: December 5, 1983

REFERENCES

1. J. H. CLEMMONS, P. G. JASIEN, AND C. E. DYKSTRA, *Mol. Phys.* **48,** 631–637 (1982).
2. A. C. LEGON, D. J. MILLEN, AND F. J. MJÖBERG, *Chem. Phys. Lett.* **47,** 589–591 (1977).
3. L. W. BUXTON, E. J. CAMPBELL, AND W. H. FLYGARE, *Chem. Phys.* **56,** 399–406 (1981).
4. R. D. BROWN, F. D. GODFREY, AND D. A. WINKLER, *J. Mol. Spectrosc.* **89,** 352–355 (1981).
5. C. WENTRUP, *Tetrahedron* **27,** 1281–1286 (1971).
6. C. WENTRUP AND P. LORENCAK, unpublished results.
7. B. BAK, O. J. NIELSEN, AND H. SVANHOLT, *Chem. Phys. Lett.* **59,** 330–333 (1978).
8. B. BAK AND H. SVANHOLT, *Chem. Phys. Lett.* **66,** 387–389 (1979).
9. B. BAK AND H. SVANHOLT, *Chem. Phys. Lett.* **75,** 528–532 (1980).
10. M. C. L. GERRY, K. YAMADA, AND G. WINNEWISSER, *J. Phys. Chem. Ref. Data* **8,** 107–123 (1979).
11. K. YAMADA AND M. WINNEWISSER, *Z. Naturforsch. a* **30,** 672–689 (1975).
12. M. WINNEWISSER, *Z. Angew. Phys.* **30,** 359–370 (1970).
13. M. WINNEWISSER AND B. P. WINNEWISSER, *Z. Naturforsch. a* **29,** 633–641 (1974).
14. D. A. HELMS, M. WINNEWISSER, AND G. WINNEWISSER, *J. Phys. Chem.* **84,** 1758–1765 (1980).
15. M. WINNEWISSER, E. F. PEARSON, J. GALICA, AND B. P. WINNEWISSER, *J. Mol. Spectrosc.* **91,** 255–268 (1982).
16. J. K. G. WATSON, *in* "Vibrational Spectra and Structure" (J. R. Durig, Ed.), Elsevier, Amsterdam/New York, 1977.
17. K. YAMADA, M. WINNEWISSER, G. WINNEWISSER, L. B. SZALANSKI, AND M. C. L. GERRY, *J. Mol. Spectrosc.* **78,** 189–202 (1979).
18. H. GÜNTHER, Dissertation, Universität Tübingen, 1975.
19. A. R. EDMONDS, "Angular Momentum in Quantum Mechanics," Princeton Univ. Press, Princeton, New Jersey, 1960.
20. P. G. JASIEN AND C. E. DYKSTRA, private communication.
21. Currently accepted value in *Nucl. Phys. A* **360** (1981), taken from a comparison of *ab initio* field gradients and experimental hyperfine structures: C. T. O'Konski and T.-K. Ha, *J. Chem. Phys.* **48,** 5356–5361 (1968).
22. W. GORDY AND R. L. COOK, "Microwave Spectroscopy" (W. West, Ed.), p. 267, Interscience, New York, 1970.
23. F. F. GARDNER AND G. WINNEWISSER, *Astrophys. J. Lett.* **195,** L127 (1975).
24. H. E. MATTHEWS AND T. J. SEARS, *Astrophys. J.* **272,** 149–153 (1983).